Dalton Transactions

ROYAL SOCIETY OF CHEMISTRY

PAPER

View Article Online
View Journal | View Issue

Check for updates

Cite this: *Dalton Trans.*, 2022, **51**, 15571

Helicenic N-heterocyclic carbene copper(I) complex displaying circularly polarized blue fluorescence†

Etienne S. Gauthier,[a] Dominika Kaczmarczyk,[b] Samuel Del Fré,[b]‡ Ludovic Favereau,[a] Elsa Caytan,[a] Marie Cordier,[a] Nicolas Vanthuyne,[c] J. A. Gareth Williams,[d] Monika Srebro-Hooper *[b] and Jeanne Crassous *[a]

Received 17th June 2022,
Accepted 17th September 2022

DOI: 10.1039/d2dt01925f

rsc.li/dalton

Enantiopure copper(I) chloride complexes bearing a monodentate *N*-(carbo[6]helicenyl)–NHC ligand have been prepared and characterized experimentally and computationally. Their high stability enables the stereochemistry to be probed by X-ray crystallography and NMR spectroscopy. The resolved enantiomeric complexes emit circularly polarized blue fluorescence with g_{lum} ~1.3×10^{-3} in solution. The photophysical and chiroptical properties of these systems, with their helicene-centred origin, are similar to those of the organic helicene-benzimidazole precursor proligand, although the reverse axial chirality configuration is preferentially observed for the complex compared to the ligand.

Introduction

Among the d^{10} coinage metals that yield strongly emissive coordination complexes, copper has attracted attention due to its higher abundance and low cost compared to heavier metals. Indeed, luminescent Cu(I) complexes have been widely studied.[1] Most examples feature four-coordinate, pseudo-tetrahedral, homo- and heteroleptic Cu(I) centres bearing diphosphine and/or diimine ligands.[2] However, their luminescence may be compromised by Jahn–Teller distortions in the excited state, and the introduction of bulky ligands has generally been necessary to improve their emissivity.[3] Recently, new three- and two-coordinate Cu(I) complexes have been designed that display bright luminescence.[4] The main common feature amongst these developments is the use of N-heterocyclic carbenes (NHCs) or their parent derivatives, cyclic (alkyl)amino carbenes (CAACs), as monodentate ligands. NHCs are a well-known class of ligands, able to form stable organometallic complexes, which offer a plethora of applications in catalysis, and in biological and materials sciences.[5] For instance, their appealing tuneable emission properties[4] have recently enabled their evaluation as efficient dopants in organic light-emitting diodes (OLEDs).[4b,6] However, there are still very few chiral emissive Cu(I) complexes, and only two recent examples of enantiopure Cu–X (X = F, Cl, Br, I, BH_4, B_3H_8) molecular systems bearing a chiral menthyl–CAAC ligand that display circularly polarized luminescence (CPL).[7] Introduction of novel chiral NHC–based Cu(I) complexes is attractive for the development of circularly polarized (CP) OLEDs, a fast-growing research field for light-emitting device technology.[8]

Our group is studying the association of metallic ions with chiral π-conjugated helicenic ligands for the conception of novel architectures with strong chiroptical properties.[9,10] Recently, we demonstrated the potential of helicenic NHC ligands for the development of cyclometallated iridium(III) and rhenium(I) complexes that display long-lived CP phosphorescence.[10a,b,e] Here, we describe the first example of an enantiopure copper(I) chloride complex bearing a monodentate helicenic NHC ligand {(*P*)- and (*M*)-**1** in Fig. 1}, an air-

[a]*Univ Rennes, CNRS, ISCR – UMR 6226, F-35000 Rennes, France.*
E-mail: jeanne.crassous@univ-rennes1.fr
[b]*Faculty of Chemistry, Jagiellonian University, 30-387 Krakow, Poland.*
E-mail: srebro@chemia.uj.edu.pl
[c]*Aix Marseille University, CNRS Centrale Marseille, iSm2, 13284 Marseille, France*
[d]*Department of Chemistry, Durham University, Durham, DH1 3LE, UK*

†Electronic supplementary information (ESI) available. CCDC 2090850. For ESI and crystallographic data in CIF or other electronic format see DOI: https://doi.org/10.1039/d2dt01925f

‡Current address: Université de Lille, CNRS, UMR 8523 – PhLAM – Physique des Lasers Atomes et Molécules, F-59000 Lille, France.

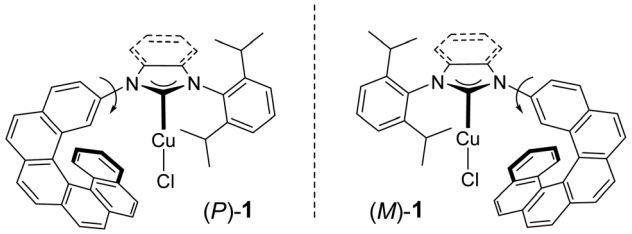

Fig. 1 Chemical structure of helicene–NHC–Cu(I) complexes (*P*)- and (*M*)-**1**.

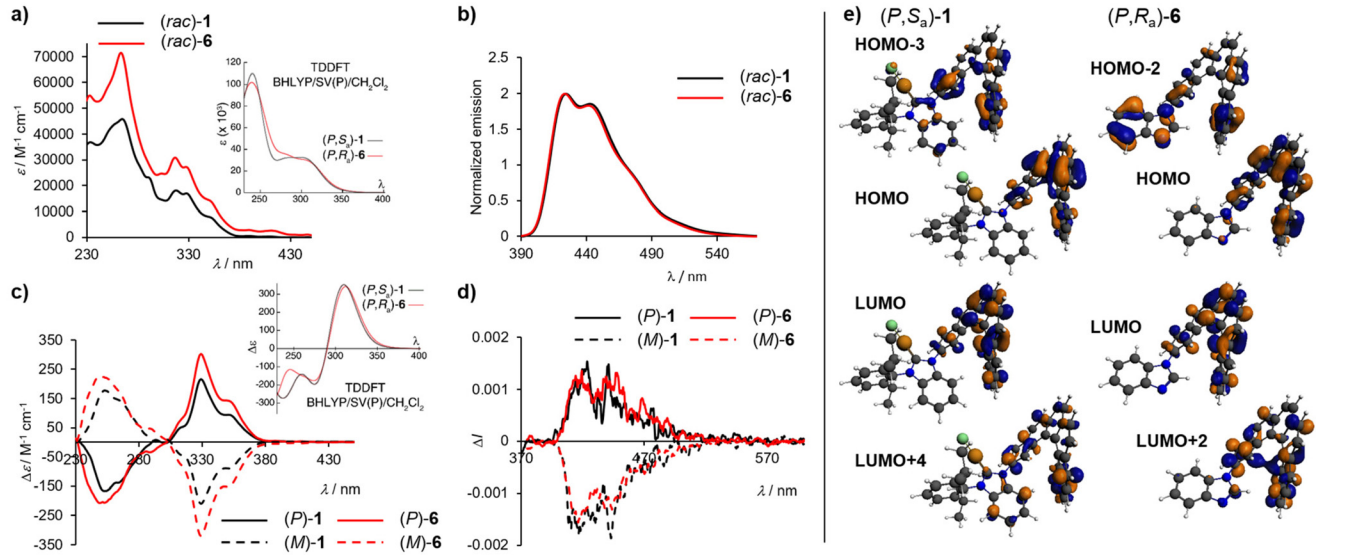

Fig. 2 Experimental (a) UV-vis, (b) fluorescence, (c) ECD and (d) CPL spectra of **1** and **6** in CH_2Cl_2 at r.t. ($C \sim 10^{-4}$ M). In the insets of (a) and (c) the corresponding simulated spectra are shown. (e) Isosurfaces (±0.04 au) of MOs involved in selected electronic transitions of (P,S_a)-**1** and (P,R_a)-**6**. See ESI† for a full set of computed data.

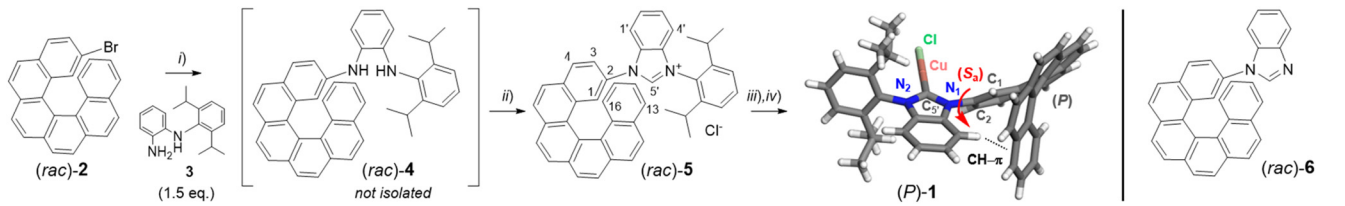

Scheme 1 Left: Synthesis of enantiopure helicene–NHC–Cu complex (*P*)- and (*M*)-**1**. (i) $Pd(OAc)_2$ (10 mol%), Xantphos (10 mol%), Cs_2CO_3 (3 eq.), dry toluene, MW, 170 °C, 30 min; (ii) conc. HCl, $(EtO)_3CH$, 85 °C, overnight (58%, two steps); (iii) CuCl (1.2 eq.), K_2CO_3 (3 eq.), acetone, 60 °C, overnight, 49%; (iv) chiral HPLC ((*S*,*S*)-Whelk-O1). X-Ray diffraction structure of (*P*)-**1** with highlighted additional (S_a) axial chirality observed in the solid state. Right: Structure of the [6]helicene-2-*N*-benzimidazole system **6**; for its synthetic details see ref. 10*e*.

and moisture-stable compound prepared in a straightforward manner from well-known 2-bromo-[6]helicene.[11] Enantiopure samples were obtained. Their photophysical and chiroptical properties (Fig. 2) have been studied experimentally and theoretically, and analysed with respect to those measured for the related [6]helicene-2-*N*-benzimidazole system (**6** in Scheme 1), prepared as reported previously.[10e] In particular, they show helicene-centred CP blue fluorescence, where the metal ion controls the axial chirality without significantly affecting the ligand-based photophysical properties. To our knowledge, this study constitutes the first example of a CPL-active, chiral NHC-based copper complex comprising a helicenic ligand.[7]

Results and discussion

Synthesis

The preparation of the helicene–NHC–Cu(I) complex (*rac*)-**1** was performed according to Scheme 1. 2,6-Diisopropylbenzene-1,2-diamine **3**, prepared *via* a 2-step literature procedure,[12a] was used in a Buchwald–Hartwig amination with racemic 2-bromo-[6]helicene (*rac*)-**2** to generate (*rac*)-**4**. The use of microwave irradiation led to efficient conversion.[13] Due to its high air- and moisture-sensitivity, (*rac*)-**4** was used directly in the subsequent cyclization with concentrated HCl and triethylorthoformate to give benzimidazolium chloride salt (*rac*)-**5**. This compound was isolated by precipitation from acetone in 58% yield after purification by silica gel chromatography. Racemic **5** was fully characterized by 1D and 2D NMR and HRMS. The appearance of the deshielded signal around 11 ppm in the ^{1}H NMR spectrum in $CDCl_3$ is characteristic of a benzimidazolium proton in close proximity to a chloride anion.[12b] Moreover, the presence of the diisopropyl groups was confirmed by the appearance of two septets for the inequivalent CH protons (δ = 2.16 and 2.00 ppm), and four doublets for the four inequivalent CH_3 protons (δ = 1.32, 1.14, 1.01 and 0.96 ppm). Typical signals from the helicenic fragment were also observed (see ESI†). In common with known helicene-based carbene precursors,[14] the helicene unit is appended onto one N atom of the benzimidazolium core, as opposed to

being a fully helical NHC precursor.[10] Note that since imidazolium cation **5** is a charged molecule, its enantiomeric resolution appeared challenging employing the classical chiral HPLC conditions we used, and was thus not considered.

With the imidazolium precursor in hand, the formation of the racemic NHC–copper(I) chloride complex **1** was achieved in 49% yield following Nolan's procedure, mixing imidazolium salt (*rac*)-**5** with copper(I) chloride and K_2CO_3 in acetone at 60 °C under air for 24 h.[15a] This method is convenient as it requires neither inert atmosphere nor addition of strong base. It shows that the NHC has good stability *in situ*, probably thanks to the steric hindrance of both helicenic and 2,6-diisopropylbenzene substituents at the N atoms. Indeed, (*rac*)-**1** was found to be stable for at least three weeks in solution in the presence of air. The absence of any signal above 9–10 ppm in the ^{1}H NMR, together with the appearance of a signal at 185.8 ppm in the ^{13}C NMR assigned to the carbenic carbon, proved the consumption of the salt **5** and formation of complex **1**. The monomeric nature of **1** was supported by HRMS. The racemic Cu(I) complex, neutral and chemically stable, was then easily resolved into pure (*P*)-**1** and (*M*)-**1** enantiomers by HPLC separation over a chiral (*S*,*S*)-Whelk-O1 stationary phase (see ESI†). Note that the additional signals appearing in the HPLC and NMR spectra of **1** are probably due to (dynamic) atropisomeric epimerization processes (see below).

Experimental and theoretical structural characterizations

Single crystals of (*P*)-**1** were grown by slow evaporation of *n*-pentane over a dichloromethane solution. Enantiopure complex (*P*)-**1** crystallized in the non-centro-symmetric $P2_12_12_1$ space group. The X-ray structure (Scheme 1) confirmed that the metallation occurs at the carbenic position, with the Cu–$C_{5'}$ distance of 1.888 Å being typical of a Cu–C(NHC) bond.[15b] The complex is monomeric in the crystal, displaying only one copper(I) centre bound to a chloride ligand in a linear geometry ($C_{5'}$–Cu–Cl = 178.4°), with Cu–Cl, $C_{5'}$–N_1 and $C_{5'}$–N_2 bond lengths (2.111, 1.360 and 1.352 Å, respectively) likewise corresponding to classical values. The [6]helicene moiety displays a typical helical angle (dihedral angle between the two terminal rings) of 63.51°.[16] The diisopropylphenyl group is almost perpendicular to the benzimidazolylidene ring, with an angle of 84.5° between the mean planes of the two rings.

It is also interesting to note that two stereogenic elements are found in the solid state of **1**, *i.e.* the (*P*) helical chirality originating from the [6]helicene unit and the axial chirality around the N_1–C_2 bond with $C_{5'}$–N_1–C_2–C_1 dihedral angle of 130.67°. The latter defines an (S_a) stereochemistry, thus suggesting that the (*P*) chirality of the helicene dictates the (S_a) axial chirality. This chiral induction is reinforced by the presence of a CH-π interaction between one CH of the benzimidazole ring and the terminal phenyl ring of the helicene (Scheme 1, H–centroid distance of 2.628 Å). Notably, the (*M*,R_a)-/(*P*,S_a)-**1** enantiomeric pair of diastereoisomers also appears to be stable in solution. Indeed, in the ^{1}H NMR spectrum, $H_{1'}$ proton of the benzimidazolylidene unit occurs as the most shielded doublet at 6.28 ppm and displays strong NOESY correlations with H_1 and H_3 (due to the proximity of benzimidazolylidene with the inner ring of helicenic unit linked to N_1). Clear NOESY correlations are also observed between $H_{1'}$ and H_{13}, H_{14}, H_{15}, thus suggesting a preferential orientation of this proton towards the outer helicenic aromatic ring. This conclusion was further supported by density functional theory (DFT) calculations involving geometry optimizations with the TPSS functional, D3 dispersion corrections, and a continuum CH_2Cl_2 solvent model (see ESI† for computational details, additional calculated results and their analysis).

Based on the results of the performed DFT geometry optimizations, the molecule of the complex **1** comprising (*P*)-[6]helicene fragment can adopt up to three stable conformations (see Fig. 3). Two of them correspond to (*P*,S_a) stereochemistry and differ in the position of the helicenic moiety relative to the metal–NHC-based fragment: the one labelled in Fig. 3 as (*P*,S_a)-**1** resembles that found in the X-ray crystal structure of the compound, in which the helicene terminal rings are placed perpendicularly to the NHC-based ligand with a visible CH-π contact between $C_{1'}H_{1'}$ of the benzimidazole ring and the outer phenyl ring of the helicene; the other, (*P*,S_a)-**1′**, lacks such interaction and instead exhibits parallel-like arrangement between the helicene terminal rings and NHC fragment. The third rotamer found was assigned to be of (*P*,R_a) configuration, and, as it shows parallel-like helicene/NHC arrangement analogous to (*P*,S_a)-**1′**, it is referred to as (*P*,R_a)-**1′** here. Note that no other (*P*,R_a) structure is possible for **1** due to steric hindrance of the Cu–Cl group. As shown in Table S2.1,† which displays results of the electronic energy evaluation of these three structures obtained with different exchange–correlation density functionals, at the standard DFT + D3 level of theory, there is visible energetic preference for the (*P*,R_a)-**1′** and (*P*,S_a)-**1′** structures, with a very slight dominance of the former (see also Fig. 3). The structure (*P*,S_a)-**1** demonstrates uniformly higher energy (by *ca.* 3–4 kcal mol^{-1}). Accordingly, based on the reported DFT + D3 energy differences, one may expect **1** to exist in solution as an equimolar mixture of both atropisomeric diastereomers. However, as the experimental NMR studies on **1** showed clear NOESY correlations between hydrogen atom $H_{1'}$ of the benzimidazole ring and hydrogen atoms H_{13}, H_{14}, H_{15} of the outer phenyl ring of the helicene fragment, the large (>5 Å) distances between these atoms found in the computed geometry of (*P*,R_a)-**1′** (see Table S2.4†) indicate that the presence of this structure in solution is not predominant. Both computed (*P*,S_a) structures, *i.e.* (*P*,S_a)-**1** and (*P*,S_a)-**1′**, could lead to the observed ^{1}H–^{1}H homonuclear correlations, and particularly (*P*,S_a)-**1**, for which all the corresponding H–H distances are well below 5 Å, fits well in the NMR analysis. Furthermore, only for this structure was the correct reproduction obtained of the experimental trends in ^{1}H and ^{13}C NMR chemical shifts for benzimidazolylidene $H_{1'}$ *vs.* $H_{4'}$ (more shielded for the former) and $C_{1'}$ *vs.* $C_{4'}$ (less shielded for the former), as seen from Table S2.5.† Note that due to rather high deviations between experimental and calculated chemical shifts values, the trends can be analysed only in a qualitative manner. All this supports the experimental conclusion on a

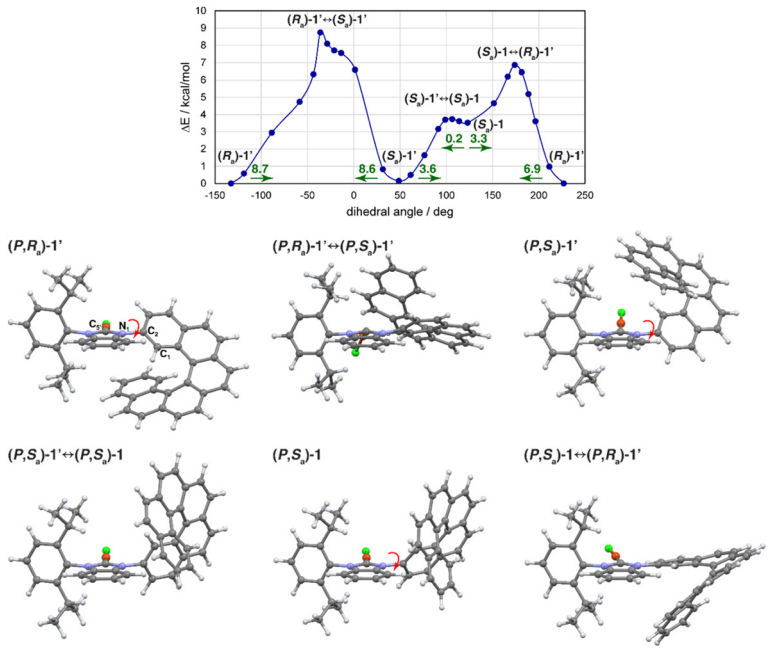

Fig. 3 Energy profile for the rotation around the N_1(NHC)–C_2(helicene) bond in the helicene–NHC–Cu complex **1** (top, to increase legibility, helicene stereochemistry designation (*P*) has been omitted in the structures' labels) along with molecular structures corresponding to its characteristic points (bottom). Numbers listed along arrows displayed in the chart are estimated energy barriers (in kcal mol^{-1}) of the transition between two adjacent minima in the direction indicated by the arrow. Based on TPSS + D3/TZVP calculations with continuum solvent model for dichloromethane.

preferential orientation of the benzimidazole ring proton $H_{1'}$ towards the outer helicenic aromatic ring in (*P*,S_a)-**1**. Moreover, this simultaneously indicates that the energy assessment of (*P*,S_a)-**1** compared to (*P*,R_a)-**1′** and (*P*,S_a)-**1′** using the standard DFT + D3 approach with continuum solvent model might be underestimated due to, for example, inaccurate description of non-covalent interactions within the typical DFT methods as a result of their inability to properly account for the long-range dynamic correlation, and/or the neglecting of explicit solvent molecules that could hinder the rotation of the helicene fragment towards structure (*P*,S_a)-**1′**. However, although the (*P*,S_a)-**1** structure is clearly dominant in solution, the calculations of the energy profile for the full rotation of the helicene unit with respect to the benzimidazolylidene fragment in **1**, *i.e.* around the N_1–C_2 axis which enabled the energetic barriers for the (S_a) ↔ (R_a) conformational chirality transformation to be assessed (see Fig. 3), indicate that the epimerization process towards (*P*,R_a) absolute configuration is definitely probable along with interconversion between both stable (*P*,S_a) rotamers. Accordingly, some co-existence of (*P*,R_a)-**1′** and (*P*,S_a)-**1′** atropisomers with the dominant (*P*,S_a)-**1** configuration may be expected in solution of **1** at room temperature.

A very similar situation, *i.e.* the presence of both helical and axial chirality within a preferential conformation, was found previously in the organic scaffold of [6]helicene-2-*N*-benzimidazole **6**, but with a preference for (*M*,S_a)/(*P*,R_a) stereochemistry with $H_{imidazole}$ pointing towards the terminal ring of the helicenic core and establishing an intramolecular CH···π interaction.[10e] It should be highlighted here, however, that as for **1**, some presence of other stereoisomers cannot be completely ruled out in solution, as the rotation around the 2-N (N_1–C_2) bond is probably not fully blocked but under an equilibrium of the epimerization process shifted toward one major configuration. Indeed, the performed DFT geometry optimizations indicated that the molecule of the ligand **6** based on (*P*)-[6] helicene fragment can adopt up to four stable conformations demonstrating rather small energetic differences (see Table S2.1†) confirmed by the results of double-hybrid functional energy evaluation (expected to give the most accurate values)[17] and rather low values of energetic barriers for the (R_a) ↔ (S_a) conformational chirality transformations as determined by the calculations of the energy profile for the full rotation of the helicene unit with respect to the benzimidazole fragment, *i.e.* around the N_1–C_2 axis (see Fig. 4). Two of these structures correspond to (*P*,R_a) and two to (*P*,S_a) stereochemistry with each pair differing in the position of the helicenic moiety relative to the benzimidazole unit. Again, the labels without the prime symbol, (*P*,R_a)-**6** and (*P*,S_a)-**6**, were assigned to the structures demonstrating CH···π interaction, and the labels with the prime symbol, (*P*,R_a)-**6′** and (*P*,S_a)-**6′**, refer to conformers lacking such contacts. Note that the (*P*,R_a)-**6** geometry resembles that found in the X-ray crystal structure of the compound, while (*P*,S_a)-**6** along with (*P*,R_a)-**6′** and (*P*,S_a)-**6′** are analogous to those obtained for **1**. Nevertheless, the calculations corroborate the aforementioned experimental assignment regarding the dominant structure of **6** *via*: (i) energetic preference of the (*P*,R_a) geometries, (ii) overall higher energetic barrier for the (R_a) → (S_a) atropisomeric transformations indicating that this compound preferentially occurs in (*P*,R_a) absolute configuration (*i.e.* as (*P*,R_a)-**6** and (*P*,R_a)-**6′**), and (iii) satis-

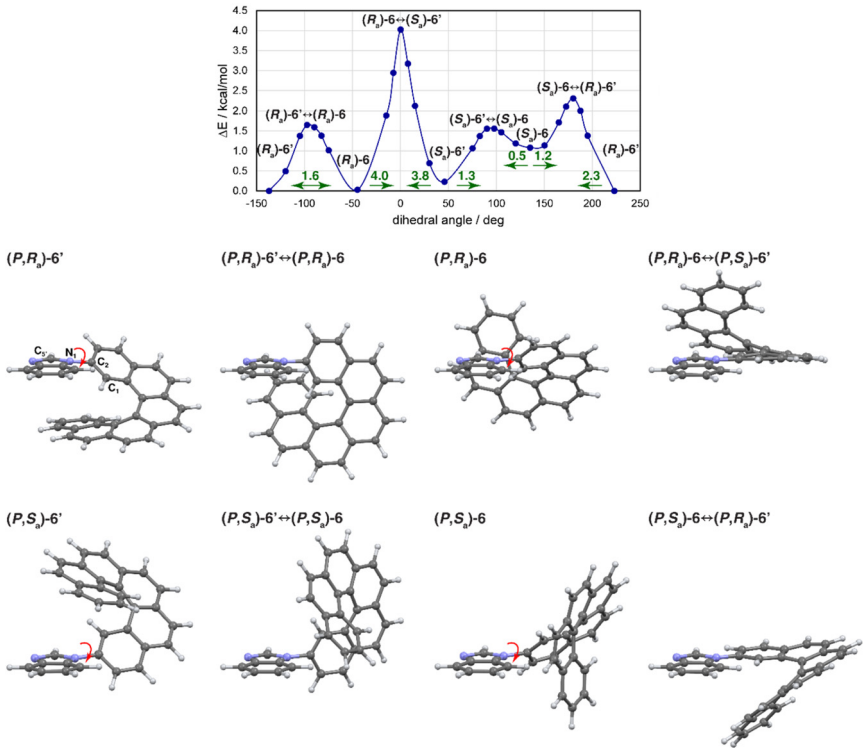

Fig. 4 Energy profile for the rotation around the N_1(imidazole)–C_2(helicene) bond in the helicene–benzimidazole ligand **6** (top, to increase legibility, helicene stereochemistry designation (*P*) has been omitted in the structures' labels) along with molecular structures corresponding to its characteristic points (bottom). Numbers listed along arrows displayed in the chart are estimated energy barriers (in kcal mol^{-1}) of the transition between two adjacent minima in the direction indicated by the arrow. Based on TPSS + D3/TZVP calculations with continuum solvent model for dichloromethane.

factory reproduction of the NMR analysis obtained for the (*P*, R_a)-**6** geometry (reported in ref. 10*e*, see Tables S2.2 and S2.3†) with a strongly shielded NMR signal computed for $H_{imidazole}$, and $H_{5'}$–H_1 and $H_{1'}$–H_3 distances consistent with the experimentally observed ^1H–^1H homonuclear correlations.

Taken together, these observations indicate that not only does the metal in **1** have the effect of stabilizing the parent NHC ligand, but it also controls the axial chirality of the resulting system, reversing it with respect to the organic analogue. This demonstrates an important role of non-covalent interactions in determining the preference for an axially chiral configuration and its rotameric structure. Note that configurationally stable, axially chiral copper(I)–NHC complexes have been used in enantioselective catalysis.[18] Furthermore, helicene–boranil systems displaying a similar kind of axial atropoisomerism have been recently described by us.[19]

Photophysical characterizations

The absorption and emission properties of **1**, and of **6** for comparison, were examined both experimentally and computationally *via* time-dependent DFT (TDDFT) calculations. In the UV-vis spectrum of **1** in CH_2Cl_2 (Fig. 2a), one can note the presence of structured bands of high intensity associated with the π-conjugated system: (i) three intense bands at 233 nm (ε ~37 000 M^{-1} cm^{-1}), 264 (46 000) and around 291 (23 000), (ii) two signals of similar intensities at 318 and 327 (18 000) followed by a shoulder around 351 (7800), and (iii) two bands of lowest energies at 390 and 410 (500). Compound **6** displays very similar absorption bands but with higher intensities (around 1.3–1.4 times stronger). The calculations reproduce these data in a satisfactory manner (Fig. 2a and ESI†), demonstrating almost the same spectral envelopes for both **1** and **6**, although with a clear discrepancy as far as relative peak intensities are concerned that might be due to a deficiency in the employed computational protocol[20] and/or to the non-negligible presence of other diastereoisomers in solution. Indeed, the calculations seem to indicate that while energetic characteristics of photophysical and chiroptical properties of **1** and **6** are rather hardly affected by the relative arrangement of the helicene and NHC–Cu or benzimidazole fragments, their intensity visibly depends on the rotameric structure of the system (for a more detailed discussion, see ESI†). An analysis of the dominant excitations of the simulated spectra shows that the observed absorption is dominated by the intense π–π* excitations within the [6]helicenic unit, accompanied by some NHC–Cu–Cl → helicene and helicene → NHC charge-transfer (CT) contributions at high energies in the case of **1**, and benzimidazole → helicene CTs at both low and high energies in the case of **6** (see Fig. 2e and ESI† for isosurfaces of involved MOs and detailed analysis). However, the overall importance of

these types of transitions is weak compared to the helix-based π–π* ones, which explains why helicene-benzimidazole **6** and helicene–NHC–Cu complex **1** display similar absorption features.

Complex **1** exhibits structured blue luminescence at room temperature (r.t.) in CH_2Cl_2 solution (Fig. 2b and ESI†), with the (0,0) vibrational component at 418 nm and a vibronic progression of around 1200 cm^{-1}. The high energy, small Stokes shift and short lifetime of 5.1 ns of this emission, together with the absence of any significant quenching by oxygen, are indicative of fluorescence as opposed to phosphorescence, whilst the vibrational structure suggests that the singlet excited state responsible is one of predominantly ligand-centred character. In a frozen glass at 77 K, the fluorescence is only marginally shifted to higher energy, but is now accompanied by intense structured phosphorescence at lower energy, $\lambda(0,0)$ = 524 nm. The long lifetime of the phosphorescence, of 960 ms, similarly points to a triplet excited state of primarily ligand-centred nature, in which spin–orbit coupling to promote the formally forbidden $T_1 \rightarrow S_0$ radiative transition is inefficient. The r.t. emission spectrum of **6** is displayed in Fig. 2b and is essentially superimposable with that of complex **1**, confirming further that the π–π* transitions within the organic scaffold are dominating the spectra. The experimental emission assignments for **1** were further confirmed with TDDFT calculations (BHLYP functional, a continuum CH_2Cl_2 solvent model, see ESI†) that demonstrate that $S_1 \rightarrow S_0$ fluorescence as well as $T_1 \rightarrow S_0$ phosphorescence correspond predominantly to LUMO → HOMO transitions, with both orbitals representing the extended π-electron system of the helicene moiety. Unsurprisingly, practically the same results, in terms of both emission energies and characteristics, including the origin, were also computed for the ligand **6** (see ESI†).

From recent investigations, it is increasingly understood that the luminescence features of such complexes are governed by the relative orientation and electronic communication between the NHC and the ancillary ligands connected by the copper in a linear fashion.[4] In some instances, the S_1–T_1 energy gap is sufficiently small to facilitate thermally activated delayed fluorescence (TADF),[4c–e] while in another, dual fluorescence and phosphorescence is observed even at room temperature.[4f] In the present case, an S_1–T_1 gap of around 5000 cm^{-1} can be estimated from the (0,0) components of the fluorescence and phosphorescence bands, which is clearly too large for TADF to occur. Though not sufficient to promote room-temperature phosphorescence, the spin–orbit coupling in **1** apparently favours formation of the triplet state from the singlet (given the higher intensity of the phosphorescence relative to fluorescence at 77 K). Competitive $S_1 \rightarrow T_1$ intersystem crossing probably then accounts in no small part for the rather low quantum yield of 1.8% for the fluorescence at room temperature.

Chiroptical characterizations

The chiroptical properties, namely optical rotation (OR), electronic circular dichroism (ECD), and CPL, were also investigated. High OR in CH_2Cl_2 was measured for both enantiomers of **1** with values similar to [6]helicenic organometallic derivatives {(*P*)-**1**: $[\Phi]_D^{25}$ = +8580 ± 5%; CH_2Cl_2, C ~4.4 × 10^{-4} M}.[16] The ECD spectra of the enantiomeric complexes are mirror-images of one another and exhibit an alternation of bands of opposite signs, diagnostic of a [6]helicenic system,[16] confirmed further by their close similarities to those recorded for the parent ligand **6** (Fig. 2c). For example, (*P*)-**1** displays a first negative band, broad and non-structured, centred at 254 nm ($\Delta\varepsilon$ = −165 M^{-1} cm^{-1}) followed by a couplet of bands with opposite signs between 293 and 300 nm with low intensities ($\Delta\varepsilon$ = +8 and −2, respectively). Finally, the last band centred at 330 nm is positive and of high intensity ($\Delta\varepsilon$ = 210) with little structure. The (*P*)-**6** enantiomer shows very similar features, although with slightly stronger intensity. The simulated[21] spectra (Fig. 2c and ESI†) agree satisfactorily with the experimental ones; as in the case of the UV-vis spectra, the results obtained for (P,S_a)-**1** and (P,R_a)-**6** structures established as likely dominant in solutions do not, however, reproduce the intensity trend seen experimentally. An MO-pair analysis of the intense excitations for both **1** and **6** indeed reveals a predominant involvement of the helicene π-system in the ECD-active transitions (see ESI† for details) that explains the close resemblance between the ECD spectra of these two systems and carbo[6]helicene (see Fig. S1.8†). This is also illustrated by the high absorption dissymmetry factors (g_{abs}) values that are typical of helicenes (see Fig. S1.7†).

Finally, the CPL activity of **1** and **6** was measured in CH_2Cl_2. The enantiomers of both compounds display a similar, significant CPL signal with a mirror-image signature {positive for (*P*) and negative for (*M*)} (Fig. 2d), and the vibrational progression can be discerned. The luminescence dissymmetry factor g_{lum} for (*P*)-**1**/(*M*)-**1** is +1.4 × 10^{-3}/−1.3 × 10^{-3} at 420 nm, while that for (*P*)-**6**/(*M*)-**6** is negligibly different, +1.3 × 10^{-3}/−1.5 × 10^{-3} at 430 nm, in line with the same electronic π-helicene-centred origin of the signal confirmed by computations (see ESI†). Magnitudes of g_{lum} for the helicene–NHC–Cu complex **1** are relatively close to values of the CAAC–Cu–menthyl complex recently reported by Ung and co-workers,[7a] with the difference that in our case the complex displays blue fluorescence arising from the helicenic unit, whereas for the CAAC-based system the signal was concluded to be phosphorescence. The phosphorescent nature of the emission in that complex has been further confirmed here *via* TDDFT calculations that revealed also its predominantly Cu–Cl origin. These results clearly show a dominant role of the helicenic NHC ligand, and helicene moiety in particular, in determining photophysical and chiroptical properties of the corresponding Cu(I) complex.

Conclusions

In conclusion, we have shown that an NHC, *N*-substituted with a [6]helicene, can be readily used to prepare enantiopure two-coordinate copper(I) complexes. They display stable helical and axial (M,R_a) and (P,S_a) stereochemistries and CPL originating from an excited state of predominantly helicene-centred char-

acter, as confirmed by the calculations. The close similarity of photophysical and chiroptical properties of these complexes with those for the helicene-benzimidazole parent system reveals that the main role of the metal fragment was to stabilize the parent NHC ligand and to control the axial chirality of the resulting system, as no direct involvement in the underlying electronic transitions was demonstrated. The system enriches the structural diversity of CPL-active, chiral NHC-based copper complex and offers new perspectives for developments of novel systems with controlled stereochemistry and topology.

Conflicts of interest

There are no conflicts to declare.

Acknowledgements

We acknowledge the Centre National de la Recherche Scientifique (CNRS) and the University of Rennes. This work was supported by the Agence Nationale de la Recherche (ANR-16-CE07-0019 "Hel-NHC" grant). Part of this work has been performed using the PRISM core facility (Biogenouest©, UMS Biosit, Université de Rennes 1). M. S.-H. thanks the PL-Grid Infrastructure and the ACC Cyfronet AGH in Krakow, Poland for providing computational resources.

References

1 (*a*) D. V. Scaltrito, D. W. Thompson, J. A. O'Callaghan and G. J. Meyer, *Coord. Chem. Rev.*, 2000, **208**, 243–266; (*b*) D. R. McMillin and K. M. McNett, *Chem. Rev.*, 1998, **98**, 1201–1219.

2 A. Barbieri, G. Accorsi and N. Armaroli, *Chem. Commun.*, 2008, 2185–2193.

3 (*a*) E. M. Stacy and D. R. McMillin, *Inorg. Chem.*, 1990, **29**, 393–396; (*b*) N. Armaroli, *Chem. Soc. Rev.*, 2001, **30**, 113–124.

4 (*a*) R. Marion, F. Sguerra, F. Di Meo, E. Sauvageot, J.-F. Lohier, R. Daniellou, J.-L. Renaud, M. Linares, M. Hamel and S. Gaillard, *Inorg. Chem.*, 2014, **53**, 9181–9191; (*b*) S. Shi, M. C. Jung, C. Coburn, A. Tadle, D. Sylvinson M. R., P. I. Djurovich, S. R. Forrest and M. E. Thompson, *J. Am. Chem. Soc.*, 2019, **141**, 3576–3588; (*c*) V. A. Krylova, P. I. Djurovich, M. T. Whited and M. E. Thompson, *Chem. Commun.*, 2010, **46**, 6696–6698; (*d*) M. J. Leitl, V. A. Krylova, P. I. Djurovich, M. E. Thompson and H. Yersin, *J. Am. Chem. Soc.*, 2014, **136**, 16032–16038; (*e*) M. Elie, F. Sguerra, F. Di Meo, M. D. Weber, R. Marion, A. Grimault, J.-F. Lohier, A. Stallivieri, A. Brosseau, R. B. Pansu, J.-L. Renaud, M. Linares, M. Hamel, R. D. Costa and S. Gaillard, *ACS Appl. Mater. Interfaces*, 2016, **8**, 14678–14691; (*f*) J. Li, L. Wang, Z. Zhao, X. Li, X. Yu, P. Huo, Q. Jin, Z. Liu, Z. Bian and C. Huang, *Angew. Chem., Int. Ed.*, 2020, **59**, 8210–8217; (*g*) M. Gernert, L. Balles-Wolf, F. Kerner, U. Müller, A. Schmiedel, M. Holzapfel, C. M. Marian, J. Pflaum, C. Lambert and A. Steffen, *J. Am. Chem. Soc.*, 2020, **19**, 8897–8909.

5 (*a*) L. Mercs and M. Albrecht, *Chem. Soc. Rev.*, 2010, **39**, 1903–1912; (*b*) M. N. Hopkinson, C. Richter, M. Schedler and F. Glorius, *Nature*, 2014, **510**, 485–496; (*c*) R. Visbal and M. C. Gimeno, *Chem. Soc. Rev.*, 2014, **43**, 3551–3574; (*d*) C. A. Smith, M. R. Narouz, P. A. Lummis, I. Singh, A. Nazemi, C.-H. Li and C. M. Crudden, *Chem. Rev.*, 2019, **119**, 4986–5056.

6 (*a*) D. Di, A. S. Romanov, L. Yang, J. M. Richter, J. P. H. Rivett, S. Jones, T. H. Thomas, M. Abdi Jalebi, R. H. Friend, M. Linnolahti, M. Bochmann and D. Credgington, *Science*, 2017, **356**, 159–163; (*b*) R. Hamze, J. L. Peltier, D. Sylvinson, M. Jung, J. Cardenas, R. Haiges, M. Soleilhavoup, R. Jazzar, P. I. Djurovich, G. Bertrand and M. E. Thompson, *Science*, 2019, **363**, 601–606.

7 (*a*) M. Deng, N. F. M. Mukthar, N. D. Schley and G. Ung, *Angew. Chem., Int. Ed.*, 2020, **59**, 1228–1231; (*b*) E. E. Braker, N. F. M. Mukthar, N. D. Schley and G. Ung, *ChemPhotoChem*, 2021, **5**, 902–905.

8 (*a*) D.-W. Zhang, M. Li and C.-F. Chen, *Chem. Soc. Rev.*, 2020, **49**, 1331–1343; (*b*) B. Doistau, J.-R. Jiménez and C. Piguet, *Front. Chem.*, 2020, **8**, 555.

9 (*a*) N. Saleh, C. Shen and J. Crassous, *Chem. Sci.*, 2014, **5**, 3680–3694; (*b*) J. OuYang and J. Crassous, *Coord. Chem. Rev.*, 2018, **376**, 533–547; (*c*) E. S. Gauthier, R. Rodríguez and J. Crassous, *Angew. Chem., Int. Ed.*, 2020, **59**, 22840–22856.

10 (*a*) N. Hellou, M. Srebro-Hooper, L. Favereau, F. Zinna, E. Caytan, L. Toupet, V. Dorcet, M. Jean, N. Vanthuyne, J. A. G. Williams, L. Di Bari, J. Autschbach and J. Crassous, *Angew. Chem., Int. Ed.*, 2017, **56**, 8236–8239; (*b*) A. Macé, N. Hellou, J. Hammoud, C. Martin, E. S. Gauthier, L. Favereau, T. Roisnel, E. Caytan, G. Nasser, N. Vanthuyne, J. A. G. Williams, F. Berrée, B. Carboni and J. Crassous, *Helv. Chim. Acta*, 2019, **102**, e1900044; (*c*) E. S. Gauthier, L. Abella, N. Hellou, B. Darquié, E. Caytan, T. Roisnel, N. Vanthuyne, L. Favereau, M. Srebro-Hooper, J. A. G. Williams, J. Autschbach and J. Crassous, *Angew. Chem., Int. Ed.*, 2020, **59**, 8394–8400; (*d*) N. Hafedh, L. Favereau, E. Caytan, T. Roisnel, M. Jean, N. Vanthuyne, F. Aloui and J. Crassous, *Chirality*, 2019, **31**, 1005–1013; (*e*) E. S. Gauthier, N. Hellou, E. Caytan, S. Del Fré, V. Dorcet, N. Vanthuyne, L. Favereau, M. Srebro-Hooper, J. A. G. Williams and J. Crassous, *Inorg. Chem. Front.*, 2021, **8**, 3916–3925.

11 D. A. Lightner, D. T. Hefelfinger, T. W. Powers, G. W. Frank and K. N. Trueblood, *J. Am. Chem. Soc.*, 1972, **94**, 3492–3497.

12 (*a*) J. Li, F. Liang, Y. Zhao, X.-Y. Liu, J. Fan and L.-S. Liao, *J. Mater. Chem. C*, 2017, **5**, 6202–6209; (*b*) H. V. Huynh, T. T. Lam and H. T. T. Luong, *RSC Adv.*, 2018, **8**, 34960–34966.

13 M. Jakubec, T. Beránek, P. Jakubík, J. Sýkora, J. Žádný, V. Církva and J. Storch, *J. Org. Chem.*, 2018, **83**, 3607–3616.
14 (*a*) I. G. Sanchez, M. Samal, J. Nejedly, M. Karras, J. Klivar, J. Rybacek, M. Budesinsky, L. Bednarova, B. Seidlerova, I. G. Stara and I. Starý, *Chem. Commun.*, 2017, **53**, 4370–4373; (*b*) M. Karras, M. Dąbrowski, R. Pohl, J. Rybáček, J. Vacek, L. Bednárová, K. Grela, I. Starý, I. G. Stará and B. Schmidt, *Chem. – Eur. J.*, 2018, **24**, 10994–10998; (*c*) R. Tarrieu, I. H. Delgado, F. Zinna, V. Dorcet, S. Colombel-Rouen, C. Crévisy, O. Basle, J. Bosson and J. Lacour, *Chem. Commun.*, 2021, **57**, 3793–3796; (*d*) E. S. Gauthier, M. Cordier, V. Dorcet, N. Vanthuyne, L. Favereau, J. A. G. Williams and J. Crassous, *Eur. J. Org. Chem.*, 2021, 4769–4776.
15 (*a*) O. Santoro, A. Collado, A. M. Z. Slawin, S. P. Nolan and C. S. J. Cazin, *Chem. Commun.*, 2013, **49**, 10483–10485; (*b*) H. Kaur, F. K. Zinn, E. D. Stevens and S. P. Nolan, *Organometallics*, 2004, **23**, 1157–1160; (*c*) A. A. Danopoulos, T. Simler and P. Braunstein, *Chem. Rev.*, 2019, **119**, 3730–3961.
16 (*a*) C.-F. Chen and Y. Shen, *'Helicene Chemistry: From Synthesis to Applications'*, Springer Berlin Heidelberg, Berlin, Heidelberg, 2017; (*b*) M. Gingras, *Chem. Soc. Rev.*, 2013, **42**, 1051–1095; (*c*) K. Dhbaibi, L. Favereau and J. Crassous, *Chem. Rev.*, 2019, **119**, 8846–8953.
17 L. Goerigk and N. Mehta, *Aust. J. Chem.*, 2019, **72**, 563–573.
18 (*a*) L. Kong, J. Morvan, D. Pichon, M. Jean, M. Albalat, T. Vives, S. Colombel-Rouen, M. Giorgi, V. Dorcet, T. Roisnel, C. Crévisy, D. Nuel, P. Nava, S. Humbel, N. Vanthuyne, M. Mauduit and H. Clavier, *J. Am. Chem. Soc.*, 2020, **142**, 93–98; (*b*) L. Kong, Y. Chou, M. Jean, M. Albalat, N. Vanthuyne, P. Nava, S. Humbel and H. Clavier, *Adv. Synth. Catal.*, 2021, **363**, 4229–4238; (*c*) M. Savchuk, L. Bocquin, M. Albalat, M. Jean, N. Vanthuyne, P. Nava, S. Humbel, D. Hérault and H. Clavier, *Chirality*, 2022, **34**, 13–26.
19 A. Macé, K. Hamrouni, E. S. Gauthier, M. Jean, N. Vanthuyne, L. Frédéric, G. Pieters, E. Caytan, T. Roisnel, F. Aloui, M. Srebro-Hooper, B. Carboni, F. Berrée and J. Crassous, *Chem. – Eur. J.*, 2021, **27**, 7959–7967.
20 M. El Sayed Moussa, M. Srebro, E. Anger, N. Vanthuyne, C. Roussel, C. Lescop, J. Autschbach and J. Crassous, *Chirality*, 2013, **25**, 455–465.
21 (*a*) M. Srebro-Hooper and J. Autschbach, *Annu. Rev. Phys. Chem.*, 2017, **68**, 399–420; (*b*) J. Autschbach, *Chirality*, 2009, **21**, E116–E152.